Comparison of Matrix Cracking in Melt-Infiltrated SiC/SiC Composites with 3D and 2D-Woven Orthogonal Architectures

Gregory N. Morscher[*]

Ohio Aerospace Institute

Brookpark, OH

ABSTRACT

Acoustic emission techniques combined with microstructural observations were used to determine the dependence of through-thickness matrix cracking (TTMC) on in-plane tensile stress for melt-infiltrated Sylramic fiber-based SiC/SiC composite panels with various 3D-woven orthogonal fiber architectures. These results were compared to prior TTMC results from similar SiC/SiC panels with 2D-woven orthogonal architectures. Both data sets were analyzed on the basis that the source for TTMC originated in the 90° or Z-fiber tows. The stress-distribution for TTMC derived for 2D composites based on the stress in the composite outside of the 0° fiber, interphase, CVI SiC "minicomposite", termed the "mini-matrix" stress, proved effective for 3D composites as well. It was found that for the 3D composites tested in the X-direction (parallel to the Z-fiber weave direction), TTMC behavior, when evaluated as a function of mini-matrix stress, was very similar to that of 2D composites with the same X-direction tow size. For the 3D composites tested in the Y-direction (perpendicular to the Z-fiber weave direction), TTMC behavior versus mini-matrix stress in the "X-Y cross-ply" or Z-fiber free regions was also very similar to the 2D cross-woven composites. However, in the "unidirectional" regions containing low fractions of Z-fibers, the onset mini-matrix stress for TTMC followed a Griffith-type relationship where the onset stress for TTMC was inversely proportional to the square root of the height

1

of the Z-fiber tows. It is shown here that the composite stress distribution needed to cause TTMC for different regions of the orthogonal 3D and 2D SiC/SiC panels could be closely predicted based on empirically-derived master curves for TTMC as a function of mini-matrix stress. The implications of these findings for SiC/SiC architecture design are discussed.

INTRODUCTION

In a companion paper [1], acoustic emission (AE) techniques were combined with microstructural observations to determine the location and the amount of matrix cracks per unit length for SiC fiber-reinforced, melt-infiltrated SiC matrix composite panels with 3D-woven X-Y-Z orthogonal architectures. These architectures had high X-Y volume fractions of the same SiC fiber type, but three different Z-direction fiber types with very low fractions. For all three Z-fiber composite systems, the matrix cracking behavior was determined for specimens tested perpendicular to the Z-fiber weave direction (Y-direction). For one 3D composite system, specimens were also tested parallel to the Z-fiber weave direction (X-direction). The AE technique enabled determination of where and how much local matrix cracking occurred in the structures with increasing stress. When tested in the Y-direction, the stress-distribution for matrix cracking differed considerably for different Z-fiber types, for the two different loading orientations, and even for the different local regions of the 3D architectures. In this paper, the stress-dependent cracking results for the 3D-woven orthogonal SiC/SiC panels are reviewed and compared with prior matrix cracking results for thin 2D-woven orthogonal SiC/SiC panels that contained the same X-Y SiC fiber types and volume fractions, and were also loaded in-plane along one of the orthogonal directions [2-3]. A cracking model previously developed to explain the 2D results is then discussed and expanded in order to account for the additional complexities introduced by the 3D architectures.

PERTINENT EXPERIMENTAL DETAILS

Details concerning the 3D orthogonal and random-stacking 2D five-harness satin woven SiC/SiC panels compared in this study and the experimental test procedures can be found in References 1 and 2. Some important details to note are as follows:

(1) Each 3D orthogonal composite had a different Z-fiber type: ZMI (Ube Industries), T300 (Amoco US), and rayon (ICF Industries), which resulted in a different Z-fiber tow thickness and fraction of Z-fiber tow content. The 3D composites will be referred to by their Z-fiber.

(2) The NASA treated Sylramic-iBN fiber tows were woven in the orthogonal (X and Y) directions for the 3D orthogonal and 2D woven composites analyzed in this study except for the rayon 3D orthogonal composite which was woven with Sylramic (Dow Corning) fiber tows in the orthogonal directions (see reference 1).

(3) The 3D orthogonal composites were not balanced. The Y-direction was woven with a standard single-tow at 7.1 or 7.9 epcm (tow ends per cm), whereas the X-direction was woven with a double tow at 3.95 epcm (which yields a net 7.9 epcm of single tows). The 2D orthogonal composites were balanced with a single-tow woven composite having 7.9 epcm and a double-tow woven composite having 3.95 epcm.

The physical properties of the 3D orthogonal and 2D woven composites are listed in Tables I and II, respectively.

For the ZMI composites, 12 mm wide by 150 mm long tensile coupons were machined out of the panels for testing in both the X and Y-directions. However, for the T300 and rayon composites, only the Y-direction orientation was tested. Note that for the Y-direction, two different regions exist within the architecture that can be examined independently by AE (see Figure 1): the

3

matrix-rich approximately unidirectional region (UNI) which contains the Z-direction tow; and the cross-ply region (XPLY) which contains a high fraction of the 90° SiC/SiC minicomposites and very little of the MI matrix.

To analyze the cracking results, it will be shown that it is important to determine the volume fractions of constituents in the 3D and 2D panels. The volume fraction of fibers in the loading or 0° direction was determined geometrically. The number of fibers per tow was 800; the fiber diameter was 10 μm; and the number of tows in the loading direction was known from the epcm. Therefore, the fiber area in the loading direction could be determined for each tensile coupon and divided by the cross-sectional area used for the determination of stress. The reason for this approach to fiber volume fraction was because some of these specimens had various surface undulations, especially the 3D specimens; and thus it was imperative that the stress-value used in the analysis correspond to the actual number of fibers in the loading direction. After the fiber fraction was determined, the volume fractions of the BN interphase, CVI SiC, SiC particles, and Si were determined from the constituent weight gain data provided by the composite manufacturer[*] (see Appendix A).

ANALYSIS

Tensile stress-strain curves for the different 3D and 2D composites are shown in Figure 2. Note that unload-reload tensile tests were performed, but the unload-reload portions were removed for clarity. The 2D composites displayed significantly greater ultimate strength than the 3D composites even though the ZMI and T300 3D-orthogonal panels were fabricated with the same fiber-type and had similar if not greater volume fraction of fibers in the X-Y directions as the 2D panels. It is currently unclear why the 3D panels were weaker than the 2D panels, but is of concern and under investigation. However, the main interest in this study pertains to the area where matrix cracking occurs, i.e., just before, at, and after the observation of non-linearity in the stress-strain curve. As shown in

---

[*] General Electric Power Systems Composites, Newark DE

Figure 2, the stress-range where significant non-linearity occurred varied considerably for different load orientations, different Z-direction fiber-types, and size of the Z-fiber tow.

2D COMPOSITE MATRIX CRACKING

In a prior study concerning TTMC in similar 2D melt-infiltrated SiC/SiC composites [2-3], it was shown that an important parameter controlling cracking is the effective stress acting on the 90° tows that exist in the matrix-rich regions outside of the 0° mini-composites (hereafter termed the "mini-matrix" region). This mini-matrix stress, $\sigma_{mini\text{-}matrix}$, can be determined from simple rule-of-mixtures theory:

$$\sigma_{mini\,matrix} = \frac{(\sigma_c + \sigma_{th})}{E_c}\left(\frac{E_c - f_{mini}E_{mini}}{1 - f_{mini}}\right) \tag{1}$$

where σ_c is the applied composite tensile stress, σ_{th} is the residual compressive stress in the matrix determined from the hysteresis loops of the tensile test [2,4], and E_c is the composite elastic modulus measured from the tensile stress-strain curve. For a balanced 2D architecture, the volume fraction of 0° minicomposites, f_{mini}, is half the total fraction of fiber, BN, and CVI SiC within the composite. The elastic modulus of the mini-composites, E_{mini}, can be estimated via the rule-of-mixtures from the elastic moduli of each constituent of the mini-composite ($E_f \approx$ 380 GPa, $E_{BN} \approx 60$ GPa, and $E_{CVI\text{-}SiC} \approx 425$ GPa) and the volume fraction of each constituent in the loading direction. Appendix A describes how this was accomplished for the 3D composites. Table II lists similar data for the 2D composites.

For the 2D panels [2, 3], Fig. 3a shows stress-strain behavior for a wide variety of constituents. Initial matrix cracking in 2D composites occurs in the 90° tows in the form of "tunnel cracks" [5-7]. As stress is increased, tunnel cracks propagate into the matrix and will propagate through-thickness if the stress is sufficient [7]. Though tunnel cracking creates a significant number of very low-energy AE events at relatively low stress [8], the majority of the cumulative AE

energy (~ 70%) occurs for a relatively small number of events (less than 10%). These high-energy events are caused by large fiber-bridged matrix cracks and result in the dramatic increase in AE energy with increasing stress [8]. Figure 4 depicts the relationship between AE energy and matrix cracking. The number of TTMC has been shown to be nearly directly proportional to the normalized cumulative energy for a number of different 2D SiC/SiC composite systems [2, 3,10]. Therefore, the stress-distribution for TTMC can be estimated from the normalized cumulative AE energy data taken during the tensile test (Figure 3b) multiplied by the final crack density measured from polished sections of the tensile specimens after the test (Figure 3c) [2-3]. Then by plotting the estimated crack density versus the calculated mini-matrix stress for each 2D system, one obtains a master-curve relationship that describes TTMC for SiC/SiC 2D-woven orthogonal composites over a wide range of constituent variation (see Figure 3d). As described in the following, these same procedures and methods of analyses were also applied to the 3D composites and then used to compare the 3D TTMC behavior against that of their companion 2D composites.

3D X-DIRECTION ORIENTED and 2D DOUBLE-TOW WOVEN COMPOSITES

TTMC density versus composite tensile stress is shown in Figure 5a for X-direction testing of the ZMI 3D composite and the 2D double-tow composite. The crack density was determined from the normalized cumulative AE activity (see Figure 9 in Reference 1) multiplied by the through-thickness crack density measured on the specimen surface after ultimate failure. It was already shown in Reference 1 that the stress-distribution for matrix cracking in the X-direction was much narrower than that in the Y-direction. This same narrow stress-distribution was also observed for 2D double-tow composites [2]. This similarity suggests that the narrow stress-distribution is dependent on the 0° or 90° tow size in some way, e.g., height of the 90° tow, number of bridging fibers in a tow, etc. However, Figure 5a shows that the stress-range where matrix cracking occurs was significantly lower for the 3D composite than for the 2D composite by about 40 MPa in applied composite stress.

6

When the X-direction crack density results for the ZMI 3D and 2D double-tow composites are plotted versus mini-matrix stress, Figure 5b shows that the data for the most part are identical with the exception of the saturation crack density for each specimen. This data collapse into one master curve is the same type of result, except with a narrower stress-distribution and lower stress-range for cracking, obtained for the various 2D single tow composites (see Fig. 3d). The very narrow character of the Figure 5b behavior is similar to traditional composite theory, where the matrix is considered to have an infinite Weibull modulus and matrix cracking occurs at a critical matrix cracking stress [9].

It should also be noted that low-stress, low-energy AE activity associated with tunnel cracking, occurred at much lower absolute and mini-matrix stresses for the 3D composite. These lower stress events in the 3D composite were probably caused by the very wide Z-bundle perpendicular to the loading direction.

3D Y-DIRECTION ORIENTED COMPOSITES

TTMC in the Y-direction of the 3D panels was observed to be significantly different than that in the X-direction. Figure 6a shows matrix crack density versus composite stress for the UNI and XPLY regions of the three different Z-fiber composites (see Figure 1b). Similar data from the single-tow 2D composite are also plotted Figure 6a. Matrix crack stress-distributions varied by over 150 MPa in composite stress for the different composites tested. The UNI regions tended to matrix crack over lower and narrower stress-ranges than the corresponding XPLY regions. The 2D composite matrix crack distribution was at a slightly higher stress-range than the "average" of all the 3D data.

Matrix crack density versus mini-matrix stress is plotted in Figure 6b for the 3D composites tested in the Y-direction as well as for the single-tow 2D composite (see Fig. 3d). The most notable feature is that the cracking in the 3D XPLY regions and the 2D composites converge somewhat, similarly to that found for the different 2D composites and for the x-direction testing (Fig. 5b). In other words, the mini-matrix stress-range where cracks form and propagate into the 0°

mini-composites is nearly the same for 3D XPLY and 2D orthogonal architectures. However, the stress-range where matrix cracking occurs in the UNI regions appears to be dependent on the tow size of the Z-fiber type; i.e., the smaller the tow size (rayon fibers), the higher the matrix cracking stress-range.

For the XPLY regions of the 3D composites that were free of Z-fiber mini-composites, a significant amount of low energy AE was observed at stresses below the onset of high-energy AE activity. This low-stress, low AE energy activity can be attributed to the formation of tunnel cracks within the 90° X-fiber tows. Tunnel cracking began at a mini-matrix stress of ~20 MPa in the XPLY regions for both the ZMI and T300 composites. However, for the rayon composite, tunnel cracking in the XPLY region began at ~60 MPa. The 90° X-direction SiC/SiC mini-composites in the rayon composites were noticeably longer and thinner than the X-direction tows in the T300 and ZMI composites. The measured maximum height for the 90° tow (see Table III) in the T300 and ZMI composites ranged from 0.08 to 0.19 mm (~ 0.14 mm on average), whereas the height for the maximum height for the 90° tow in the rayon composites ranged from 0.08 to 0.16 mm (~ 0.12 mm on average). The presence of thicker 90° tows may be the cause for the lower matrix tunnel-cracking stresses in the XPLY region of the T300 and ZMI composites. Note that for random lay-up architectures of 2D-woven composites, tunnel cracking can also occur at relatively low mini-matrix stress (< 20 MPa, see Figure 6b). For these 2D architectures, in contrast to the 3D architectures, there are often two contacting 90° tows with a combined height of up to ~0.3 mm. These regions would of course not be through the width of the specimen; however, they are prime sights for low-stress tunnel or micro-crack formation.

For the XPLY regions of the 3D and 2D composites, there exists a 20 MPa separation in mini-matrix stress between the T300 and ZMI composites and the similar rayon and 2D composites (Figure 6b). However, there was a considerable amount of estimation in the determination of mini-matrix stress for the different regions, and error is expected even in the use of processing parameters since some variation in local composite constituent composition will

occur over the entire composite panel. Nevertheless, it is possible that real TTMC differences do exist for the different XPLY regions of the 3D composites due to the thinner 90° tow height of the rayon composite resulting in smaller local areas of unbridged matrix cracks.

For the UNI regions, the lack of convergence of the TTMC stress distributions appears to be due to the lack of crack formation in the T300 and rayon 3D composites at stresses lower than those required for the ZMI composites. Crack formation in the UNI regions is likely related to the size of the Z-direction mini-composites, which act as flaws in the relatively dense matrix between the 0° mini-composites. This implies the possibility of a Griffith-type relationship between the onset for TTMC cracking and the Z-direction mini composite size or height, which is effectively the flaw size in the matrix. Assuming this to be the case, Figure 7a plots TTMC versus the inverse square root of the height of the Z-fiber tow measured 0.5 mm from the face of the composite [1] @ for both the applied composite stress and the mini-matrix stress. A linear relationship exists for both stresses, confirming this implication. This can be taken one step farther. The estimated TTMC density can be plotted versus a "stress-intensity" (applied stress versus the square root of the Z-fiber tow height) as shown in Figure 7b. At least for crack densities below ~5, the distribution of matrix cracks for all three 3D orthogonal composites converges for the "stress-intensity" parameter very well.

As described in reference 1, significant tunnel cracking for UNI regions of the ZMI composite occurred prior to TTMC (Figure 6), presumably due to the large tow height of the ZMI Z-tow. However, little if any tunnel cracking prior to TTMC occurred for the UNI regions of T300 and rayon composites.

DISCUSSION

@ h for the Z-fiber bundles was measured In reference 1 and found to be 0.4, 0.28, and 0.15 mm for ZMI, T300, and rayon composites, respectively.

The cracking model previously developed for 2D melt-infiltrated SiC/SiC panels with woven orthogonal architectures is based on the general assumption that as composite stress is increased in the $0°$ direction, the source for TTMC will originate primarily within the $90°$ minicomposites. Initial tunnel cracks that form in the $90°$ minicomposites at stresses too low for TTMC propagation are the initial sites for TTMC formation when the stress in the composite is sufficient for TTMC propagation. When cracks form in $90°$ minicomposites above the stress to propagate TTMC, the cracks do not "tunnel" to any great extent, but rather almost instantaneously propagate through-thickness. Three aspects of this cracking behavior are considered to be most significant in relation to the effect of composite architecture on matrix cracking (see figure 4): (1) the onset stress for tunnel cracking, (2) the onset stress for TTMC, and (3) the stress distribution for TTMC. As discussed in the following, these parameters are inter-related and key to the development of physics-based damage and life models for textile-woven ceramic composites in general and melt-infiltrated SiC/SiC composites in particular. With analyses of the physical factors controlling these parameters in hand, some general guidelines are offered on architecture approaches that can improve the composite stresses required for TTMC.

Onset Stress For Tunnel Cracking

Tunnel cracking has been discerned by the author, based on AE, to some degree prior to TTMC in every Syl-MI composite (over 100 different composite panels tested) that possesses orthogonal mini-composites oriented perpendicular to the loading direction, i.e., 2D woven and 3D-orthogonal in the cross-ply regions. It may not be possible to prohibit tunnel crack formation in cross-ply composites. However, tunnel cracking did not occur for the smaller T300 or Rayon Z-fiber tows in the UNI regions of the 3D orthogonal composites. Also, it appears that tunnel cracking occurred at lower stresses for the larger $90°$ size ZMI and T300 XPLY regions compared to the thinner Rayon XPLY region (reference 1). One possible implication of this result would be that the $90°$ tow

height in composites could be engineered thinner so as to increase the stress for crack initiation in the 90° bundles to a stress greater than the TTMC stress.

Onset Stress For Through-Thickness Matrix Cracking

The onset stress for TTMC is the most crucial parameter from a design standpoint. At this stress and above, depending on the temperature and environment, time-dependent strength degradation occurs due to oxidation embrittlement and/or enhanced creep of the fully-loaded 0° fibers [10].

It appears that the criterion for TTMC formation in these woven 2D and 3D systems is dependent on the stress for a tunnel crack to "break out" of the tunnel. Once a stress is achieved that enables a crack to form and propagate in the CVI SiC and/or MI (Si + SiC) matrix surrounding a 90° tow, the matrix crack cannot be stopped by bridging fibers to any great extent.

The same two extremes for the TTMC onset stress in 2D woven SiC/SiC composites were observed for the 3D orthogonal composites in regions containing 90° orthogonal tows: (1) a higher mini-matrix stress condition typical of most standard single tow woven composites and (2) a lower mini-matrix stress condition typical of double tow woven composites. The former condition has been demonstrated on composite systems that exhibit a range in the onset composite stress for TTMC of over 100 MPa due to variations in constituent fractions [2] and different fiber types [3]. The latter condition is associated with woven composites that possess a very narrow stress-range for matrix cracking. For both conditions, due to the prevalence of tunnel cracks formed at lower stresses, plenty of flaws are available for through-thickness cracking once the critical stress is attained. The reason for the difference in mini-matrix stress for the two conditions is not fully understood at the moment.

For the UNI regions of the 3D orthogonal composites the onset stress for TTMC appears to be entirely dependent on the size (height) of the Z-fiber tow and follows a Griffith-type relationship (Figure 7a). The implication is clear, the larger the Z-fiber tow size the lower the stress for matrix cracking.

11

Stress Distribution For Through-Thickness Cracking

The stress distribution for through-thickness cracking dictates the non-linear stress-strain response of the material. It is also an important parameter for intermediate temperature mechanical properties because the greater the number of matrix cracks the greater the degradation in time-dependent strength.

For stresses above the TTMC stress, matrix cracks originate in the 90° and/or Z-fiber tows and propagate through the thickness of the composite. For composites with a 90° orthogonal tow, a simple empirical model has been developed in reference 3 for single tow woven MI composites that will be applied here. The matrix crack density could be approximated based on the simple Weibull equation:

$$\rho_c(\sigma_{min\,/matrix}) = \rho_c\left[1 - \exp\left(-\left(\frac{\sigma_{min\,/matrix}}{\sigma_o}\right)^m\right)\right]$$

(3)

where $\rho_c(\sigma_{minimatrix})$ is the estimated crack density at a given stress, ρ_c is the final crack density measured after the tensile test, σ_0 would be the reference stress and correspond to the average $\sigma_{minimatrix}$ where the normalized cumulative AE energy equals 0.623, and m is the Weibul modulus. m would be the only unkown variable. For the 2D MI matrix systems woven with a single tow, it was determined [3] that σ_0 = 150 MPa and m = 5. Figures 3d and 6b show the estimated crack density from this model assuming a final crack density of 9.5 cracks/mm. There is good agreement between the model and estimated crack density up to about 5 cracks/mm. For the purpose of modeling stress-strain or elevated temperature stress-rupture properties this is sufficient since the stresses that are required to cause the higher crack densities are beyond the practical use stresses of these materials [2]. This model would suffice for the XPLY region of the Y-direction tested 3D orthogonal composites. For 2D and 3D double-tow systems, σ_0 was determined to be 77.5 MPa from the AE data and m = 12 best fit the estimated crack density data assuming a final crack density of 8.5 cracks/mm, the average of the two composites in Figure 5b. A similar approach

could be used for the UNI regions based on the stress-intensity parameter (Figure 7b).

Finally, it is of interest to note, that the rayon UNI had the highest $\sigma_{minimatrix}$ range for matrix cracking. However, the high modulus matrix carries as much load as the load-bearing minicomposites compared to the relatively low modulus of the XPLY "minimatrix" region, i.e., $90°$ bundles. This results in a lower absolute composite stress-range where matrix cracking occurs for the UNI region when compared to the XPLY region of the rayon or even T300 composite. The major differences between rayon XPLY or T300 XPLY with ZMI XPLY appear to be a higher fiber volume fraction and/or straighter load-bearing fibers with thinner $90°$ bundles in the rayon composite. This implies then, that the highest composite stress for matrix cracking may be achieved in cross-ply structures with the highest load-bearing fiber volume fraction and thinnest ply widths possible. This could be taken advantage of in local regions of component structures where high-matrix cracking stresses are desired.

It is hoped that the above analyses can be used to steer development of and/or to verify fiber-architecture property models, e.g., references 11 and 12, which can be applied generally to ceramic matrix composites formed by textile weaving. It is also anticipated that as the understanding between stress-dependent matrix cracking (as well as other properties, e.g., through-thickness strength and thermal conductivity) and local architecture grows, structures will be designed that incorporate the necessary local architectures for desired local properties in a given component.

CONCLUSIONS

The stresses at which matrix cracks occur in SiC/SiC composites with different architectures can vary dramatically. It has been shown that many factors

contribute to the stress-range for matrix crack formation and propagation: the volume fraction of fibers in the loading direction, the area of the load-bearing fiber tow, the height of any Z-direction fiber tow, the height of the 90° fiber tow (ply thickness), straightness of the fibers, and the constituent content and properties of the matrix. However, for architectures with a significant fraction of 90° tows, e.g., 2D and 3D woven composites, the stress-distribution for matrix cracking appears primarily dependent on the average stress in the part of the matrix that is outside the load-bearing minicomposites. For unidirectional regions of composites, matrix cracking stresses could be very large, but insertion of Z-direction tows perpendicular to the loading direction causes matrix cracks to propagate at lower stresses. For practical purposes, the highest composite stresses for matrix crack propagation occurred for cross-ply regions in 3D orthogonal architecture. The model applied here suggests that this is due to the lower effective modulus and stress in the region of the matrix outside of the load-bearing minicomposite. Perhaps future architecture designs can be formulated to take advantage of this phenomenon for local high-applied stress regions in CMC components.

APPENDIX A: ESTIMATION OF LOCAL ELASTIC MODULUS FOR Y-DIRECTION 3D ORTHOGONAL COMPOSITES

In order to determine the stress on the matrix outside of the fiber, BN, CVI SiC minicomposite, the elastic moduli of the UNI (E_{UNI}) and XPLY (E_{XPLY}) regions had to be estimated. The approach taken was to estimate E_{UNI} from rule-of-mixtures (ROM) based on the volume fractions that made up the UNI region. Then, the contribution of E_{XPLY} could be estimated or "backed out" from the measured E_c assuming a serial link-up (Reuss estimate) of the UNI and XPLY regions [13].

The fraction of fibers in the X and Y-directions was determined from the fiber area in the loading direction divided by the measured tensile specimen area from the simple relationship (note that specimen width would be in the numerator and denominator and therefore cancels itself out):

14

$$f_{XorY} = \frac{N_{ply}N_f \pi R_f^2 (epmm)}{t}$$ (A1)

where N_{ply} is the number of plies or layers of woven fiber, N_f is the number of fibers in a tow (800 for Sylramic), R_f is the fiber radius, epmm is ends per mm converted from epcm, and t is the thickness of the tensile specimen. The Z-direction bundle fiber fraction, f_Z, in the UNI region was determined from the geometry of the weave. The total volume fraction of fiber, f_{TOT}, would then be the sum of f_X, f_Y, and f_Z.

The starting weight of the sized fiber architecture and subsequent weight gains of each constituent, i.e., CVI BN, CVI SiC, α-SiC particles, and molten Si, were known from the manufacturer. Therefore, the absolute weight was known for the interphase and matrix constituents. The volume of the interphase and matrix constituents was determined from the weight gains and densities. The densities used for SiC, Si, and BN were: 3.2, 2.33, and 1.5 [14] g/cc, respectively. The total fraction of interphase and matrix constituents was assumed to be $1 - f_{TOT}$. Then the fractions of each constituent could be determined from absolute volume of each constituent divided by the total volume of BN and matrix constituents multiplied by $1 - f_{TOT}$.

It was assumed that CVI BN and CVI SiC deposition occurred uniformly on the fiber-structure to form the CVI SiC skeletal "preform". The fraction of X, Y, and Z-direction minicomposites, f_{mini-X}, f_{mini-Y}, and f_{mini-Z}, respectively, was determined from the addition of the proportional fractions of BN and SiC to the respective orientation of fiber:

$$f_{mini-i} = f_i + \frac{f_i}{f_{Tot}}(f_{BN} + f_{CVI-SiC})$$ (A2)

---

* The interphase weight gain was slightly greater than the weight gain used here because sizing removal was not taken into account. The sizing was approximately 0.2% of the fiber weight. For the rayon composite, fiber decomposition during initial heating would also add to the true weight gain of the BN.

where i is X, Y, or Z. The elastic modulus of the minicomposite was then determined from ROM for each constituent of the minicomposite (E_{SYL} = 380 GPa, $E_{CVI\ SiC}$ = 425 GPa, and E_{BN} = 60 GPa).

Next, the fraction of fiber, interphase, CVI SiC preform within the UNI region and the XPLY region was determined. The UNI region consisted of Y-direction and Z-direction minicomposites, the XPLY region consisted of Y-direction and X-direction minicomposites. Therefore, the fraction of CVI SiC preform in each region would simply be the sum of the fractions of minicomposite contained within each region. The thickness and width of a tensile bar are the same for both UNI and XPLY regions. Therefore, the volume of the UNI and XPLY regions depends on the length of the region. The lengths of the UNI and XPLY regions were estimated from the average measured lengths of X-direction minicomposites (w_x in Figure 1b) and spaces between X-direction minicomposites (u_y in Figure 1b). On average, the lengths were nearly identical for the T300 and ZMI composites, ~ 1.45 mm. However, for the Rayon composite, the length of the XPLY region was "longer" on average, w_x ~ 1.6 mm, than the length of the UNI region, u_y ~ 1.3 mm, because the X-direction tows were longer and thinner on average for the rayon composite compared to the T300 and ZMI. Therefore, the fraction of CVI SiC preform within each region was determined from:

$$f_{preform-UNI} = f_{mini-Y} + f_{mini-Z}\left(\frac{w_x + u_Y}{2u_Y}\right)$$ (A3)

and

$$f_{preform-XPLY} = f_{mini-Y} + f_{mini-X}\left(\frac{2w_x}{w_x + u_Y}\right)$$ (A4)

for the UNI and XPLY regions, respectively.

The fraction of MI matrix ($\square$-SiC + Si) within each region was then simply determined from the fraction of the volume that is not CVI SiC preform:

$$f_{MI-UNI} = 1 - f_{preform-UNI}$$ (A5)

16

$$f_{MI-XPLY} = 1 - f_{preform-XPLY} \qquad\qquad (A6)$$

The elastic moduli of the UNI and XPLY regions can now be estimated. First, the elastic modulus of the MI region was estimated from the rule-of-mixtures:

$$E_{MI} = \left(\frac{f_{\alpha-SiC} E_{\alpha-SiC} + f_{Si} E_{Si}}{f_{\alpha-SiC} + f_{Si}} \right) \qquad\qquad (A7)$$

where $E_{\square-SiC}$ and E_{Si} are 460 and 300 GPa, respectively. Then, assuming that the composition of Si and $\square$-SiC particles in the MI part of the matrix is the same throughout the architecture, the elastic modulus of the UNI region can be estimated from ROM:

$$E_{UNI} = f_{mini-Y} E_{mini-Y} + f_{mini-Z} E_{mini-Z} + f_{MI-UNI} E_{MI} \qquad\qquad (A8)$$

E_{mini-Z} is expected to be very low. Also, f_{mini-Z} is relatively small; therefore, it was assumed that the quantity $f_{mini-Z} E_{mini-Z}$ in equation A8 was zero. The estimated elastic modulus of the XPLY region, E_{XPLY}, was then "backed out" from the Reuss estimate of two elements in series:

$$E_{XPLY} = \left(\frac{w_x + u_y}{E_c} - \frac{u_Y}{E_Y} \right)^{-1} w_x \qquad\qquad (A9)$$

E_{XPLY} was estimated to be 183, 175, and 188 GPa for rayon, T300, and ZMI composites, respectively (Table I).

REFERENCES:

1. G.N. Morscher, H.M. Yun, and J.A. DiCarlo, "Matrix Cracking in 3D Orthogonal Woven SiC Fiber Reinforced Melt-Infiltrated SiC Matrix Composites," submitted to J. Am. Ceram. Soc.

2. G.N. Morscher, "Stress-Dependent Matrix Cracking in 2D Woven SiC-fiber Reinforced Melt-Infiltrated SiC Matrix Composites," submitted to *Comp. Sci. Tech.*

3. G.N. Morscher, "Matrix Cracking in Four Different 2D SiC/SiC Composite Systems," SAMPE (2003) in print

4. M. Steen and J.L. Valles, ASTM STP 1309, M.G. Jenkins et al., Eds. American Society for Testing and Materials, West Conshohocken, PA, 1997, pp. 49-65

5. Z.C. Xia and J.W. Hutchinson, "Matrix Cracking of Cross-Ply Ceramic Composites," *Acta metal. mater,* **42** [6] 1933-45 (1994).

6. J-M. Domergue, F.E. Heredia, and A.G. Evans, "Hysteresis Loops and the Inelastic Deformation of 0/90 Ceramic Matrix Composites," *J. Am. Ceram. Soc.,* **79** [1] 161-70 (1996)

7. B.N. Cox and D.B. Marshall, "Crack Initiation in Fiber-Reinforced Brittle Laminates," *J. Am. Ceram. Soc.,* **79** [5] 1181-88 (1996)

8. G.N. Morscher, "Modal Acoustic Emission Source Determination in Silicon Carbide Matrix Composites," in Review of Progress in Quantitative Nondestructive Evaluation, eds. D.O. Thompson and D.E. Chimenti, CP 509, American Institute of Physics, pp. 383-390 (2000)

9. J. Aveston, G.A. Cooper, and A. Kelly, "Single and Multiple Fracture: The Properties of Fiber Composites," pp. 15-24 in The Properties of Fibre Composites, Conference Proceedings, National Physical Laboratory (Guildford, U.K.). IPC Science and Technology Press, Ltd., Teddington, U.K., 1971

10. G.N. Morscher, J.Z. Gyekenesi , and R.T. Bhatt, "Damage Accumulation in 2-D Woven SiC/SiC Ceramic Matrix Composites," in Mechanical, Thermal and Environmental Testing and Performance of Ceramic Composites and

Components, ASTM STP 1392, M.G. Jenkins, E. Lara-Curzio, and S.T. Gonczy, Eds., pp. 306-319 (2000)

11. B.N. Cox, W.C. Carter, and N.A. Fleck, "A Binary Model of Textile Composites – I. Formulation," Acta metal. mater. 42 [10] 3463-3479 (1994)

12. B.N. Cox and R.M. McMeeking, "The Binary Model – User's Guide", Edition 2.1 December, 2002

13. T.K. Ishikawa, K. Bansaku, N. Watanabe, Y. Nomura, M. Shibuya, and T. Hirokawa, "Experimental Stress/Strain Behavior of SiC-Matrix Composites Reinforced with Si-Ti-C-O Fibers and Estimation of Matrix Elastic Modulus," *Comp. Sci. Tech.*, **58** [1] 51-63 (1998)

14. S.K. Mital, M. Tong, P.L.N. Murthy, and J.A. DiCarlo, "Micromechanics-Based Modeling of Thermal and Mechanical Properties of an Advanced SiC/SiC Composite Material," NASA/TM – 97-206295 December, 1997

Table I: Some Measured and Estimated Physical Properties of Y-direction Oriented 3D-Orthogonal Composites

Physical Property	Rayon	T300	ZMI
t, mm	1.95	1.75	2.05
f_X	0.160	0.178	0.152
f_Y	0.203	0.226	0.174
f_Z	0.001	0.014	0.032
$f_{CVI\ BN}$	0.073	0.078	0.045
$f_{CVI\ SiC}$	0.238	0.194	0.236
$f_{\alpha\text{-SiC}}$	0.185	0.173	0.208
f_{Si}	0.139	0.137	0.143
$f_{mini\text{-}X}$	0.297	0.294	0.272
$E_{mini\text{-}X}$, GPa	374	--	--
$f_{mini\text{-}Y}$	0.377	0.373	0.310
$E_{mini\text{-}Y}$, GPa	359	355	372
$f_{mini\text{-}Z}$	0.002	0.023	0.057
$f_{preform\text{-}UNI}$	0.422	0.396	0.368
$f_{preform\text{-}XPLY}$	0.880	0.961	0.853
$f_{MI\text{-}UNI}$	0.578	0.604	0.632
$f_{MI\text{-}XPLY}$	0.121	0.039	0.147
E_{UNI}, GPa	378	368	392
E_{XPLY}, GPa	183	175	188
σ_{th}, MPa	45	42	40

Table II: Some 2D Composite Properties

Property	2D Single-tow woven	2D Double-tow woven
f	0.190	0.191
f_{BN}	0.074	0.065
$f_{CVI\ SiC}$	0.234	0.218
f_{mini}	0.343	0.332
E_{mini}	361	363
E	228	197
σ_{th}	57	50

Table III: 3D Architecture Average Dimensions

Z-direction Fiber-type	$w_{x,}$ mm	$h_{x,}$ mm	$w_{y,}$ mm	$h_{y,}$ mm	$u_{y,}$ mm	$u_{x,}$ mm
ZMI	1.50	0.14	0.97	0.12	1.45	0.45
T300	1.54	0.14	0.94	0.12	1.44	0.30
Rayon	1.62	0.12	0.94	0.10	1.34	0.30
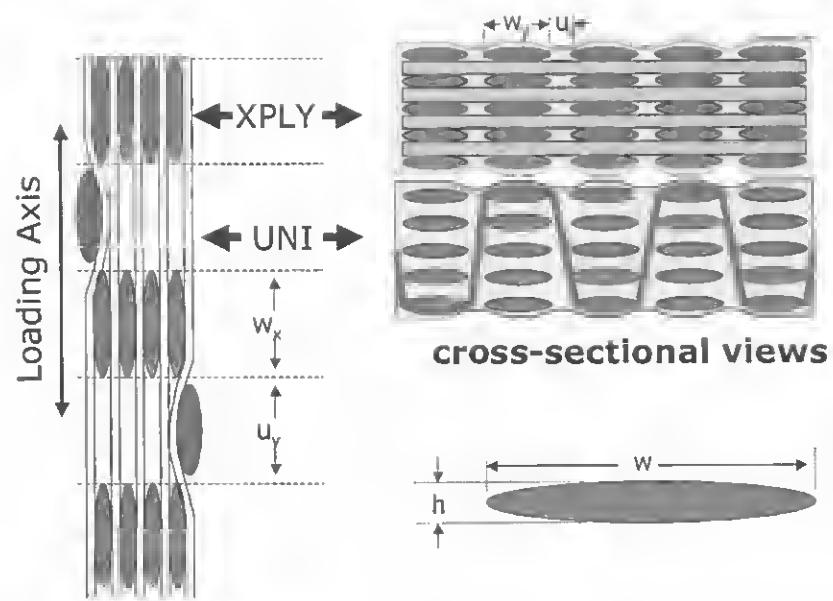
Figure 1: Schematic representation of the 3D orthogonal composite aligned in the Y-direction. Note that only nine layers are represented, the composites actually contained fifteen layers as is shown in Figure 1 of reference 1, i.e., seven X-layers and eight Y-layers.
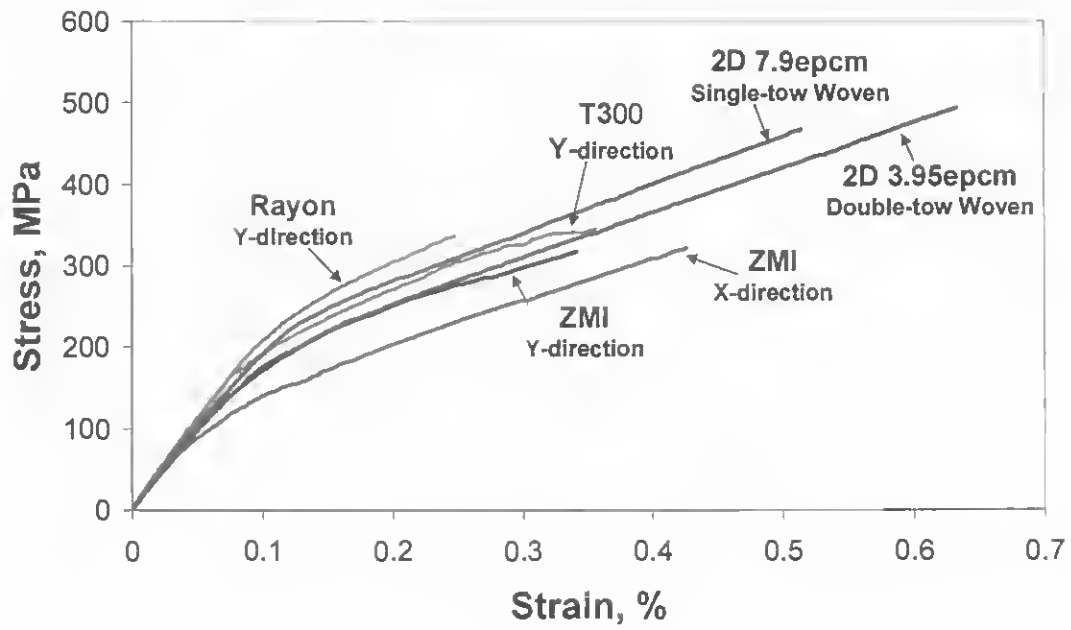
Figure 2: Stress-strain data (hysteresis loops removed)

(a)

(b)

(c)

(d)
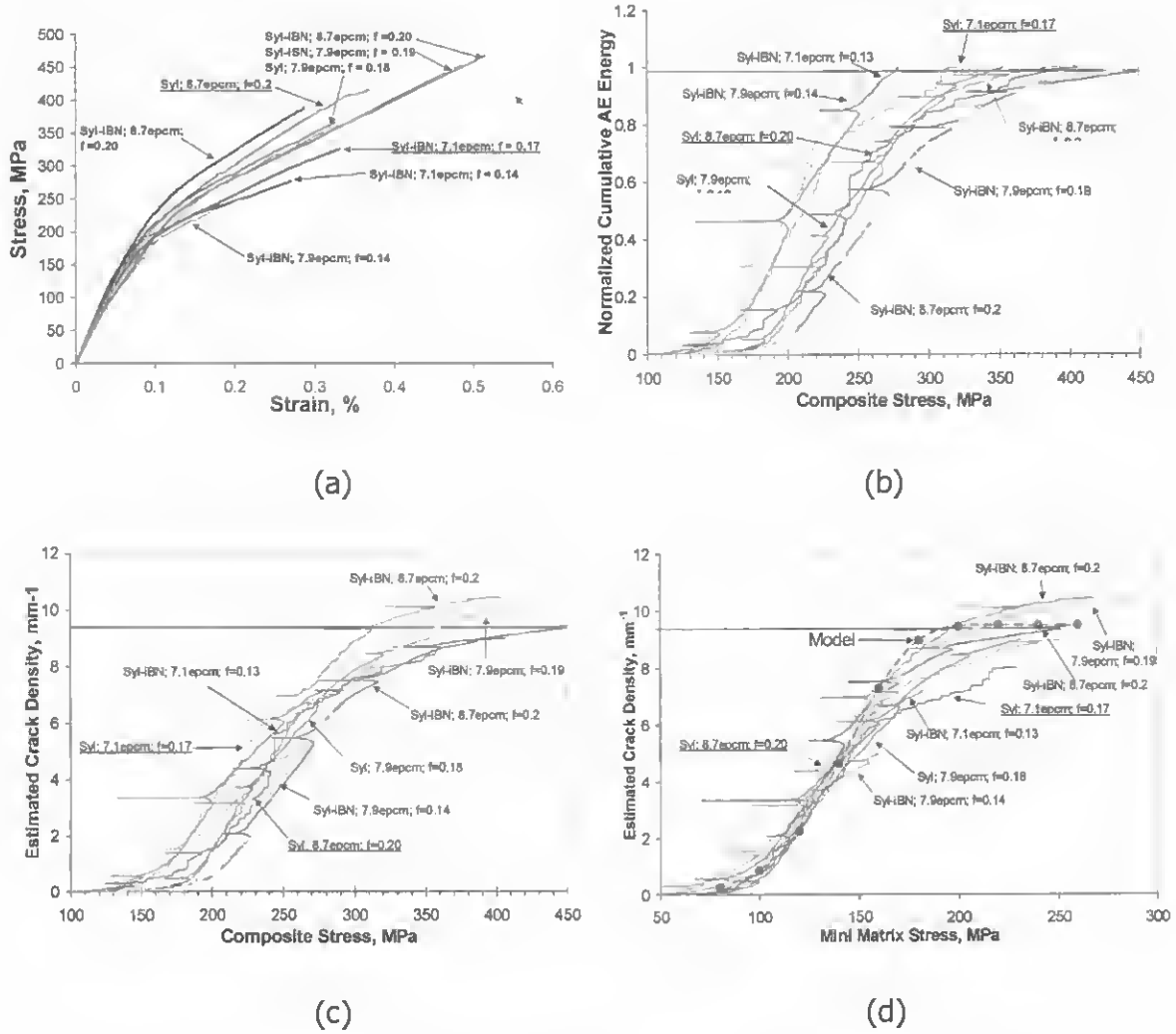
Figure 3: Data from 2D woven Sylramic reinforced melt-infiltrated SiC matrix composites [2,3]: (a) Stress-strain curves for different 2D architecture and volume fraction composites, (b) normalized cumulative AE energy versus applied stress, (c) Estimated crack density versus applied stress, and (d) Estimated crack density versus $\sigma_{minimatrix}$. The data labels that are not underlined are from reference 2 and the data labels that are underlined are from reference 3. Each specimen is from a different composite panel.
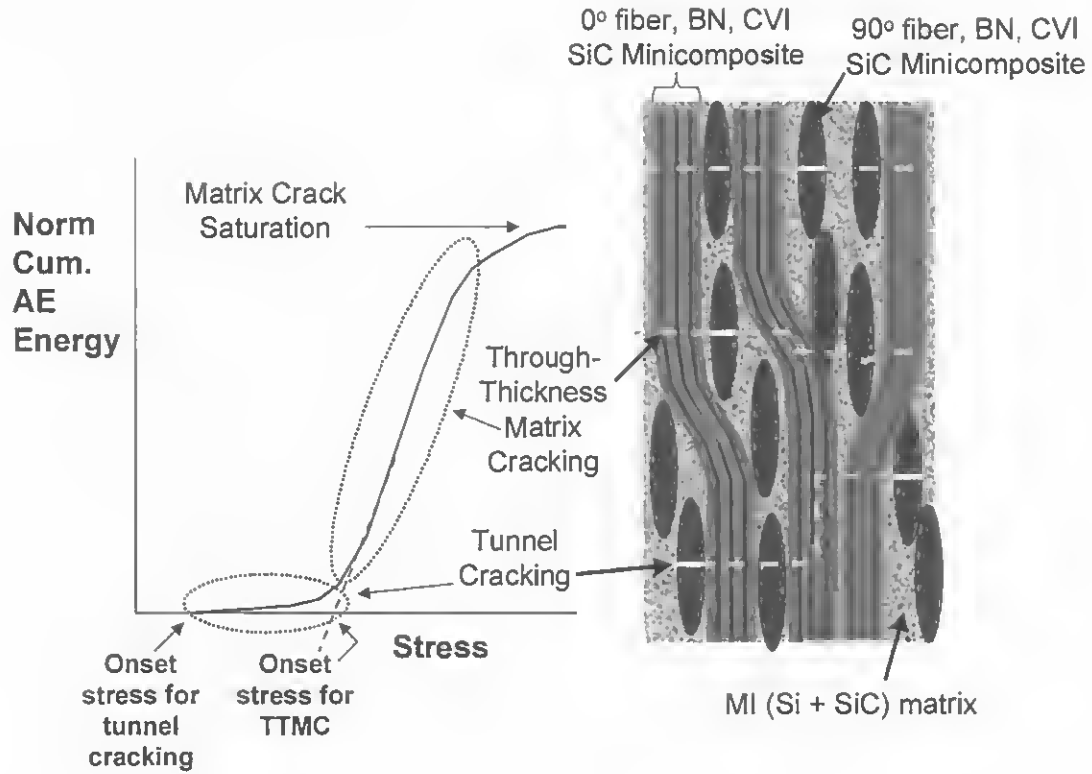
Figure 4: Schematic representation of typical AE and relation to tunnel and through-thickness matrix cracking.
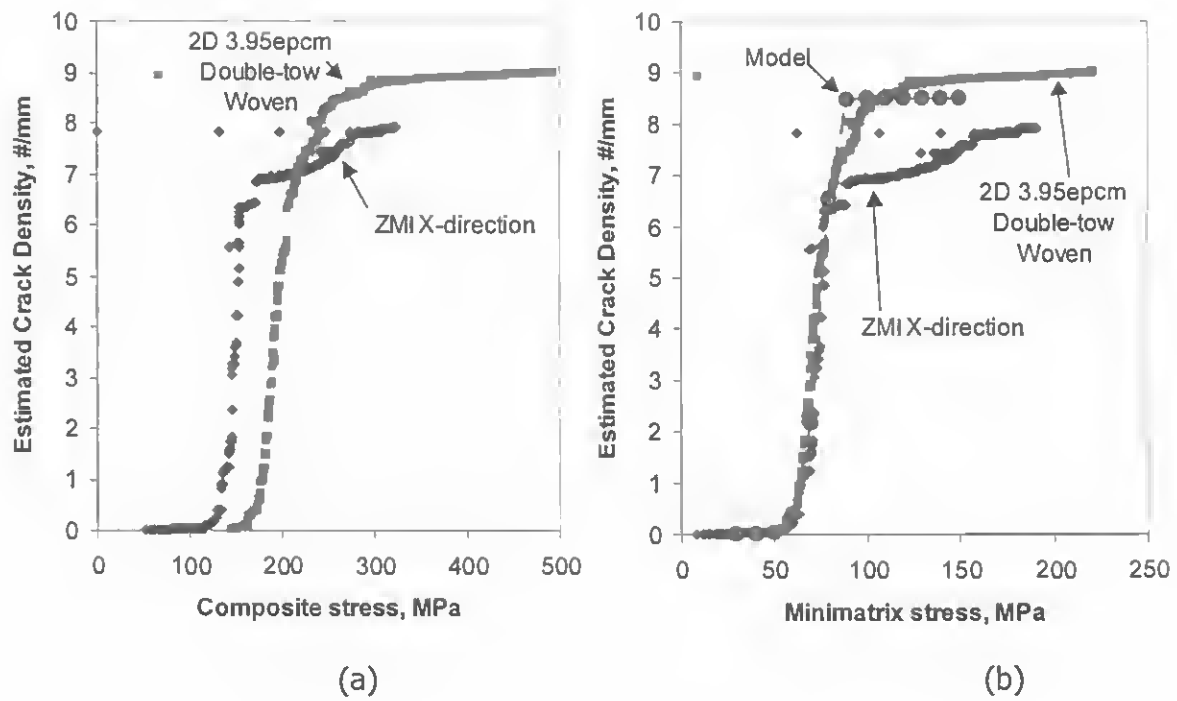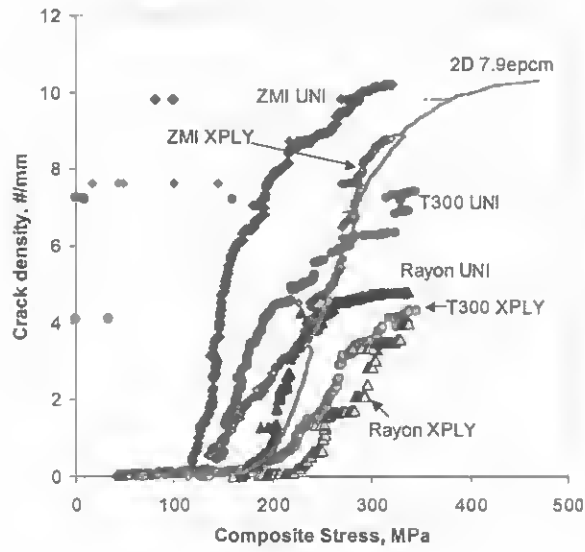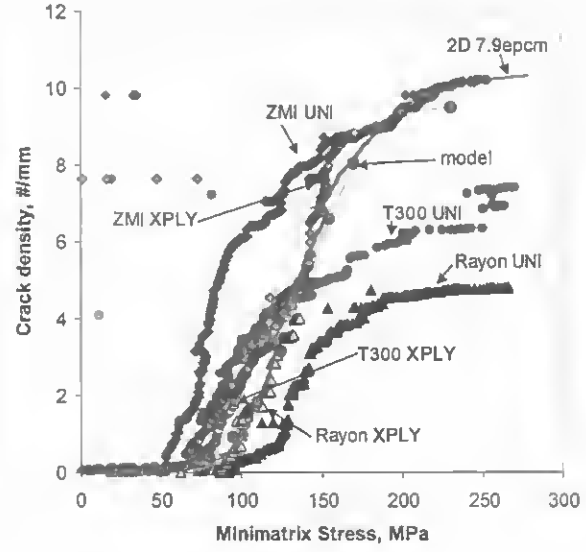
Figure 5: Estimated matrix crack density versus (a) composite stress and (b) mini-matrix stress for composites with a double-tow woven in the loading-direction.
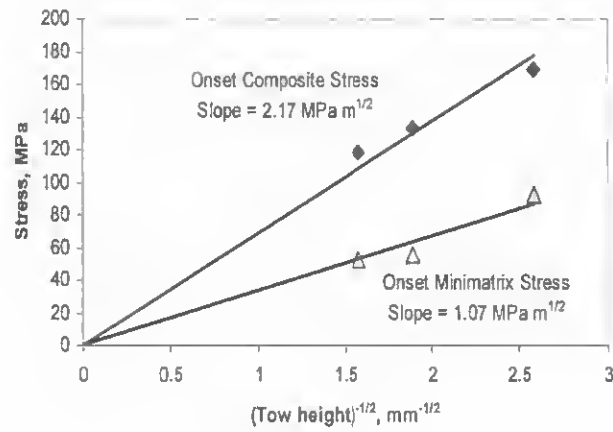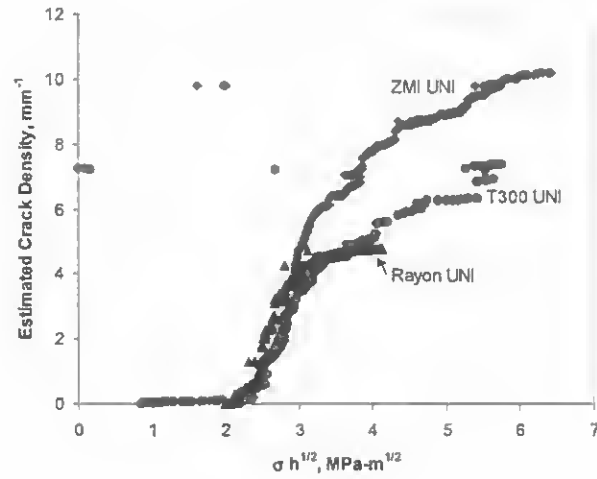
Figure 6: Estimated crack-density, based on AE activity, for the two regions of Y-direction composites.

(a)

(b)

Figure 7: (a) Onset stress for TTMC versus the square root of the inverse tow height of the Z-direction tow for the UNI regions of the 3-D Orthogonal composites. (b) Estimated crack density for UNI regions versus "stress-intensity".